Rare Metal Materials and Engineering
Volume 55, Issue 11, November 2026
Available online at www.rmme.ac.cn

Science Press

Cite this article as: Du Juan, Bao Shengzhong, Yang Shaodan, et al. Corrosion Behavior of Pre-oxidized 56Cu-22Ni-12Fe-8Al-2La Anode Alloy in High-Temperature Molten Electrolyte for Aluminum Electrolysis[J]. Rare Metal Materials and Engineering, 2026, 55(11): 2756-2764. DOI: https://doi.org/10.12442/j.issn.1002-185X.20250607.

ARTICLE

Corrosion Behavior of Pre-oxidized 56Cu-22Ni-12Fe-8Al-2La Anode Alloy in High-Temperature Molten Electrolyte for Aluminum Electrolysis

Du Juan[1,2], Bao Shengzhong[3], Yang Shaodan[1,2], Zhou Yanjun[2,4], Zhuang Yuwei[5], Cao Shuguang[1]

[1] Institute of Materials, Henan Academy of Sciences, Zhengzhou 450046, China; [2] Henan Key Laboratory of Advanced Conductor Materials, Zhengzhou 450002, China; [3] Zhengzhou Non-ferrous Metals Research Institute Co. Ltd of CHINALCO, Zhengzhou 450041, China; [4] School of Material Science and Engineering, Henan University of Science and Technology, Luoyang 471000, China; [5] High & New Technology Research Center of Henan Academy of Sciences, Zhengzhou 450046, China

Abstract: The corrosion behavior of unoxidized and pre-oxidized 56Cu-22Ni-12Fe-8Al-2La anode alloys was investigated in a Na_3AlF_6-K_3AlF_6-AlF_3-Al_2O_3 electrolyte for aluminum electrolysis at 800 °C. Electrochemical tests of the metal anodes in molten salt for aluminum electrolysis were conducted, and the corrosion mechanism of the alloys was investigated. Results show that the oxide layer formed on the pre-oxidized alloy at 800 °C in an O_2 atmosphere mainly consists of oxides of aluminum, nickel, iron, copper, and lanthanum. After aluminum electrolysis for 3 h, the corrosion products formed on the unoxidized anode alloy demonstrate a tri-layered structure, and the discontinuous and porous oxide layer provides a connected channel during electrolysis, allowing the electrolyte to directly penetrate the metal matrix to a depth of approximately 320 μm. The corrosion oxide layer formed on the pre-oxidized anode alloy is about 190 μm in thickness. The outer and inner oxide layers include continuous Ni-/Fe-/Al-/Cu-rich oxides (mainly $NiFe_2O_4$ and $CuAlO_2$). The middle layer, with a thickness of about 15 μm, contains a dense and continuous $NiFe_2O_4$ layer. A small amount of electrolyte appears in the oxide layer and penetrates into the metal matrix. The pre-oxidized alloy exhibits better corrosion resistance and stability than the unoxidized alloy during aluminum electrolysis.

Key words: Cu-Ni-Fe-Al-La alloy; metal anodes; high-temperature molten salt corrosion; aluminum electrolysis

1 Introduction

Aluminum production is usually conducted by the conventional Hall-Héroult process[1–2]. However, the high energy consumption and emission of greenhouse gases of the Hall-Héroult process have a large adverse impact on the environment[3–4]. Developing non-carbon inert anodes for aluminum electrolysis offers an effective approach to addressing this issue. Gallino[5], Yang[6], and Wang[7] et al have employed Cu-Fe-Ni and Fe-Ni alloys as inert anode materials for aluminum electrolysis. $NiFe_2O_4$-based cermets[8–10] and (Cu, Ni)/(10NiO-$NiFe_2O_4$) conducting ceramics[11–13] have also been investigated as anode materials in aluminum electrolysis. As an alternative material to carbon anodes in the modern electrolytic aluminum industry, metallic-based inert anodes exhibit several advantages, such as high strength, excellent electrical conductivity, strong resistance to thermal shock, ease of processing and shaping, and the ability to connect with metal conductor rods[14–15]. Copper- or nickel-based alloys, such as Cu-Ni-Fe[16–17], Cu-Al[18–19], and Ni-Fe[20–21], are the main metallic anode materials because of the capability of forming corrosion-resistant oxide layers during the molten salt

Received date: December 01, 2025
Foundation item: Scientific Research Start-Up Fund of Henan Academy of Sciences (231817003); Natural Science Foundation of Henan Province (242300420030); High-Level Achievement Award and Cultivation Project of Henan Academy of Sciences (20252317003); Key R&D and Promotion Special Project (Science and Technology Research) of Henan Province (242102230031); Innovation Team Project of Henan Academy of Sciences (20250104); Fundamental Research Fund of Henan Academy of Sciences (240617039)
Corresponding author: Du Juan, Ph. D., Professor-Level Senior Engineer, Institute of Materials, Henan Academy of Sciences, Zhengzhou 450046, P. R. China, E-mail: juan_du@hnas.ac.cn

Copyright © 2026, Northwest Institute for Nonferrous Metal Research. Published by Science Press. All rights reserved.

electrolysis process. The formation of a dynamically balanced, corrosion-resistant oxide layer on the anodic surface is the key point of preparing a qualified metal anode[22–23].

Beck et al[15] and Cao et al[24] demonstrated that the formation of an adherent and electronically conductive $NiFe_2O_4$ layer in the passive film after electrolytic oxygen evolution significantly enhances the corrosion resistance of Cu-Ni-Fe alloys and Ni-Fe anodes in molten fluoride salts. Helle et al[25] have studied the corrosion behavior of Cu-Al-Ni-Fe alloy in a KF-AlF_3 melt at 700 °C. The results showed that a $CuAl_2O_4$ protective layer formed on the substrate surface effectively prevents the penetration of the electrolyte and the spalling of oxides. Tian[13] and Yang[26] et al have proved that the continuous and dense $FeAl_2O_4$, $NiAl_2O_4$, $CuAl_2O_4$, or $NiFe_2O_4$ films derived from the metal phase in the cermet can provide excellent protection to the internal structure of the anode during the electrolysis process. However, the $NiFe_2O_4$ and metal aluminate protective scales are usually fragile and exhibit poor adhesion to the alloy substrates. These characteristics will rapidly lead to the failure of the anode during the aluminum electrolysis process. Therefore, improving the adhesion between the protective layer and the alloy substrate is essential to obtain stable and corrosion-resistant metal anodes during electrolysis in molten salts.

Besides, some researchers demonstrated that pre-oxidizing can also improve the corrosion resistance of the metal alloys. Wei et al[27] studied the oxidation of Ni-Fe-15Cr alloy at 960 °C in air, which exhibits a tri-layered oxide structure on the alloy surface with an outer layer of $(Ni, Fe)_3O_4$ spinel, a middle layer of $(Ni, Fe, Cr)_3O_4$ spinel, and an oxidation-resistant inner layer of Cr_2O_3. Simultaneously, the tri-layered oxide structure exhibits good electrical properties and corrosion resistance in the aluminum electrolysis process. Tamasgavabari et al[28] examined the corrosion behavior of a Ni-6Al-10Cu-11Fe-15Cr nickel-based alloy as an inert anode material in a cryolite melt. The study found that the addition of Al and Cr to the alloy plays an important role in delaying corrosion of the metal alloys by the molten salt electrolyte, due to the formation of Al_2O_3 and Cr_2O_3 after pre-oxidation. Singh et al[29] have studied Cu-Ni-Fe alloys as anodes in a low-temperature laboratory aluminum electrolysis cell. It was found that the pre-formed oxide layer remains compact after electrolysis through oxidation treatment of the alloy. However, it remains a great challenge for metal alloys to survive in the high-temperature (960 ℃) corrosion conditions of NaF-AlF_3 cryolite molten salt for a long time.

Based on the requirements above for metallic anode alloys, developing an oxide layer with superior adhesion and corrosion resistance on the anode surface is desirable for aluminum electrolysis. According to our previous study, the addition of La can pin grain boundaries and improve the oxidation resistance and adhesion of the oxide film[30]. The pre-oxidation may promote the homogenization of microstructure and the formation of an oxide layer[20]. Therefore, in this study, both the elements Al and La are added to the Cu-Ni-Fe alloy, following a pre-oxidation pretreatment. In particular, a high-temperature KF-NaF-AlF_3-based electrolyte with high alumina solubility is employed here to offer a better service condition for the metal anodes. Until now, there is limited research on the electrochemical corrosion behavior of pre-oxidized and multi-element-modified Cu-Ni-Fe alloy during aluminum electrolysis. Especially, the evolution of the pre-oxidized film and the corrosion mechanism of the Cu-Ni-Fe-Al-La alloy have not yet been revealed in the high-temperature KF-NaF-AlF_3-based electrolyte.

In this study, a pre-oxidized Cu-Ni-Fe-Al-La alloy as the anode material was prepared for aluminum electrolysis. The electrochemical performance of the pre-oxidized Cu-Ni-Fe-Al-La alloy was investigated under galvanostatic electrolysis in a Na_3AlF_6-K_3AlF_6-AlF_3-Al_2O_3 electrolyte at 800 °C. For comparison, the corrosion behavior of the Cu-Ni-Fe-Al-La alloy with and without pre-oxidation was evaluated and discussed.

2 Experiment

2.1 Sample preparation

The 56Cu-22Ni-12Fe-8Al-2La alloys were prepared from high-purity (>99.9%) Cu, Ni, Fe, and Cu-La master alloy by high-frequency induction melting under an argon atmosphere. During the melting and casting process, electromagnetic stirring was used to obtain a high-quality ingot. The test samples with a diameter of 8.5 mm and a length of 7 mm were cut from the ingot using an electrical discharge machine. Before pre-oxidation, the samples were sequentially ground with SiC paper up to 2000#, rinsed with deionized water, and ultrasonically degreased in ethanol. Finally, the dried samples were pre-oxidized at 800 °C under an O_2 atmosphere for 100 h.

2.2 Galvanostatic electrolysis and electrochemical test

For comparison, the pre-oxidized and unoxidized samples were chosen to undergo aluminum electrolysis tests in a three-electrode cell at 800 ° C for 3 h. Electrolysis tests were conducted at an anode current density of 0.5 $A \cdot cm^{-2}$ in mixed cryolite electrolyte containing NaF (20wt%), KF (20.27wt%), AlF_3 (51.74wt%), and Al_2O_3 (8wt%). A laboratory electrolytic cell was set up within a vertical furnace, as shown in Fig.1. A high-purity graphite crucible used as the cathode was placed inside a corundum crucible sealed with a stainless-steel lid.

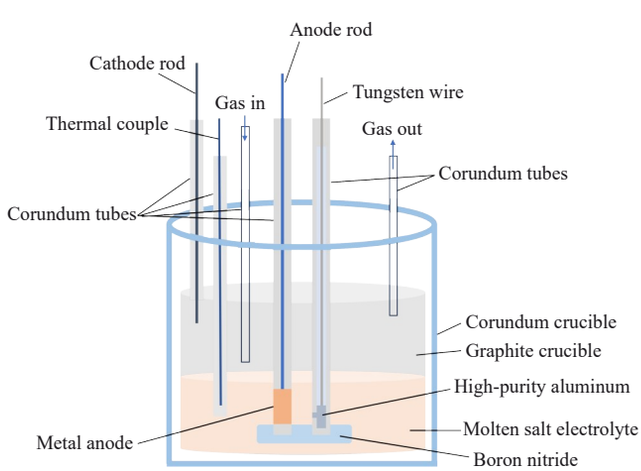


Fig.1 Schematic diagram of electrolysis cell

The stainless-steel sealing lid has gas inlet and outlet holes to allow inert gas flow. The bottom of a cylindrical anode sample (the test area with a diameter of 7.5 mm and a height of 7 mm) was threaded into a boron nitride disc, and the top of the anode sample was connected to the power supply with a corundum as a protective sleeve. High-purity aluminum in a corundum crucible with a 1.5 mm-diameter hole on the bottom was employed as the reference electrode. A tungsten wire served as the current collector for the reference electrode.

The anode and reference electrodes on the boron nitride disc were suspended above the electrolyte at the beginning of heating. The temperature of the electrolysis cell was raised to 250 °C and held for 2 h, and then heated to 800 °C at 5 °C·min^{-1} and held for 0.5 h. After the electrolyte was fully melted, the anode was lowered and immersed to a depth of 2 cm below the electrolyte surface. Open-circuit potential (OCP) was measured for 1 h by an electrochemical workstation (IM6, Zahner). Then, the galvanostatic electrolysis was conducted at a current density of 0.5 A·cm^{-2} for 3 h. During electrolysis, electrochemical impedance spectroscopy (EIS) measurements were conducted hourly with a perturbation amplitude of 10 mA and the frequency range from 5000 Hz to 0.1 Hz. Upon completion of electrolysis, the anode material was raised above the molten salt electrolyte. After cooling to room temperature under an inert gas atmosphere, the sample was retrieved for microstructural analysis. The linear sweep voltammetry curves were also measured after EIS measurement on parallel samples following the same procedures described above. The scanning range was from OCP to 2.8 V vs. Al/Al^{3+} at a scanning rate of 0.001 V·s^{-1}.

2.3 Microstructure characterization

After electrolysis, the samples were encapsulated in epoxy resin to secure the corrosion product layer against detachment. The cross-section was ground with 600#, 800#, and 1200# abrasive paper. After grinding, the samples were rinsed with deionized water and ethanol to remove residual abrasives and subsequently dried. The phase structure of the oxide layer was identified by X-ray diffractometer (XRD, PANalytical X'Pert Pro) with Cu-Kα radiation in the 2θ range of 10°–90° under conditions of 40 kV and 40 mA. The surface and cross-section morphologies of the samples after electrolysis were characterized by a scanning electron microscope (SEM, JEOL JSM-6360LV) with an energy-dispersive X-ray spectroscope (EDS, Oxford-INCA).

3 Results and Discussion

3.1 Microscopic morphology and element analysis of pre-oxidized anode alloy

Fig. 2 presents SEM image and EDS elemental analysis of the cross-section of the 56Cu-22Ni-12Fe-8Al-2La alloy after pre-oxidation at 800 °C for 100 h under an O_2 atmosphere. The results demonstrate the formation of an oxide layer extending approximately 30 μm beneath the material surface. This oxide layer is mainly composed of oxides of Al, Ni, Fe, Cu, and La. In particular, the oxide of Al is the predominant product. To some extent, the formation of this oxide layer can prevent the rapid erosion of the metal anode by the electrolyte during the initial immersion period[28,31–32].

3.2 Corrosion behavior of anode alloy in aluminum electrolysis process

3.2.1 OCP and electrolytic voltage test

For comparison, both pre-oxidized and unoxidized alloys are used as anode materials in the electrolysis experiments for electrochemical performance testing. Fig. 3a shows OCP variation for the pre-oxidized and unoxidized metal anode

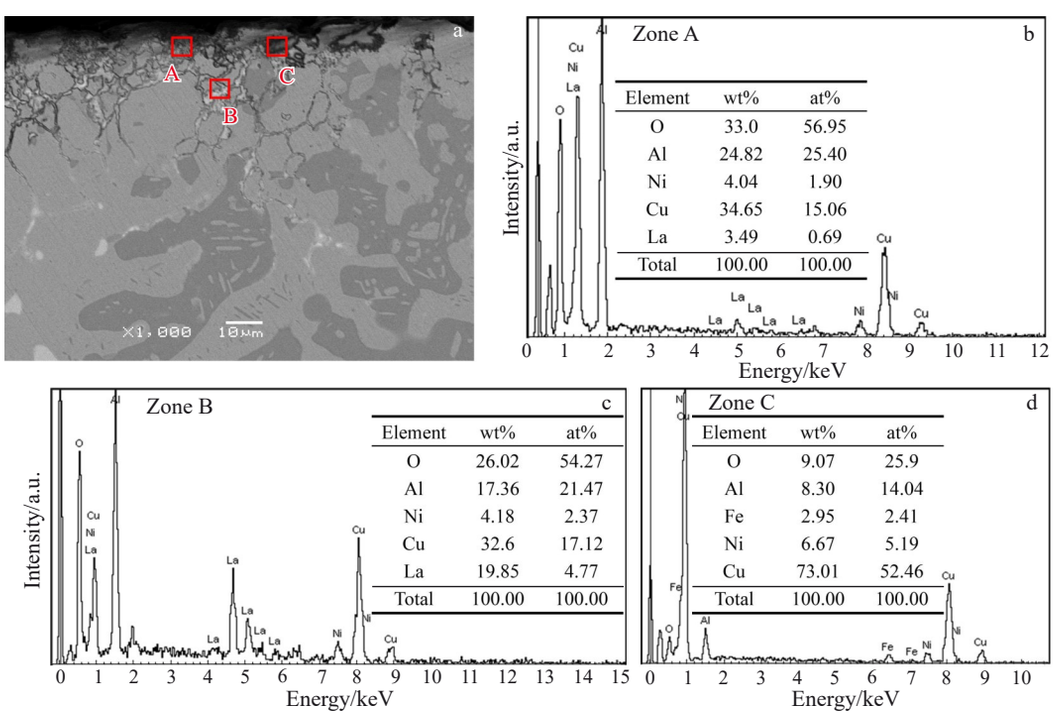


Fig.2 SEM image (a) and EDS results (b–c) of cross-section of the pre-oxidized 56Cu-22Ni-12Fe-8Al-2La alloy

materials after immersion in the electrolyte for 1 h. It demonstrates that OCP of the pre-oxidized anode alloy is significantly higher than that of the unoxidized anode alloy during the initial immersion in the electrolyte. This is mainly attributed to the formation of a pre-oxidized layer on the surface of the anode alloy. At the initial stage of immersion in the electrolyte, this pre-oxidized layer serves as a protective barrier that effectively slows down the erosion of the high-temperature electrolyte on the metal substrate.

Fig. 3b shows the electrolysis voltage as a function of electrolysis time for both anode alloys. The electrolysis voltages of both anode alloys rise sharply from a starting value of 0.4 V to 2.5 V in the first 6 min of electrolysis. This period is assumed to be dominated by the electrochemical oxidation of the anodes[33]. Subsequently, the electrolysis voltage increases slowly to around 2.7 V at the end of electrolysis, which is attributed to the fact that the anode alloys have nearly reached steady-state electrolysis. For example, a balance between the rates of oxide formation and dissolution has been established[34–35]. It is noted that the electrolysis voltage of pre-oxidized anode alloy is slightly higher by approximately 0.03 V than that of the unoxidized anode alloy after 100 min of electrolysis. The oxide layer thermally developed on 56Cu-22Ni-12Fe-8Al-2La alloy has acceptable anode resistance for the Hall-Héroult aluminum electrolysis process.

3.2.2 Corrosion product

The cross-section morphologies of the unoxidized and pre-oxidized anode metals are analyzed by SEM, as shown in Fig. 4. Clearly, both the surfaces of unoxidized and pre-oxidized anode metals are covered by a layer of solidified electrolyte. For unoxidized anode (Fig. 4a), the thickness of surface oxide is approximately 160 μm. Besides, between the metal substrate and the oxide layer, there is an electrolyte penetration zone with a thickness of approximately 320 μm, and the total thickness of the corrosion zone is about 480 μm. In comparison, the original oxide layer formed on the pre-oxidized anode alloy, which is composed of aluminum oxide, has been transformed into a dense mixed oxide layer. The thickness of mixed oxide layer is approximately 190 μm, the thickness of electrolyte penetration zone is about 130 μm, and the total thickness of the corrosion zone is about 320 μm (Fig.4b).

XRD patterns of the unoxidized and pre-oxidized anode alloys are presented in Fig. 5. It is demonstrated that the surfaces of the unoxidized and pre-oxidized anode alloys after 3 h of electrolytic corrosion mainly contain oxide (Cu_2O and NiO), spinel ($NiFe_2O_4$ and $CuAlO_2$), and potassium/sodium/aluminum fluoride (KF_3, NaF_3, and AlF_3) phases. Fig.6 briefly illustrates various phases in the oxide layers. For unoxidized 56Cu-22Ni-12Fe-8Al-2La anode alloy, as shown in Fig.6a, the surface oxide shows a tri-layered oxide structure with an outer layer of Cu oxide (mainly Cu_2O), a middle layer composed of discontinuous $NiFe_2O_4$ and Al_2O_3, and an inner layer containing porous Ni-/Fe-/Al-rich hybrid oxides. Obviously, the discontinuous, porous oxide layer forms a connected channel during electrolysis, allowing direct contact between the electrolyte and the anode metal matrix. This eventually leads to the formation of electrolyte penetration zones with a

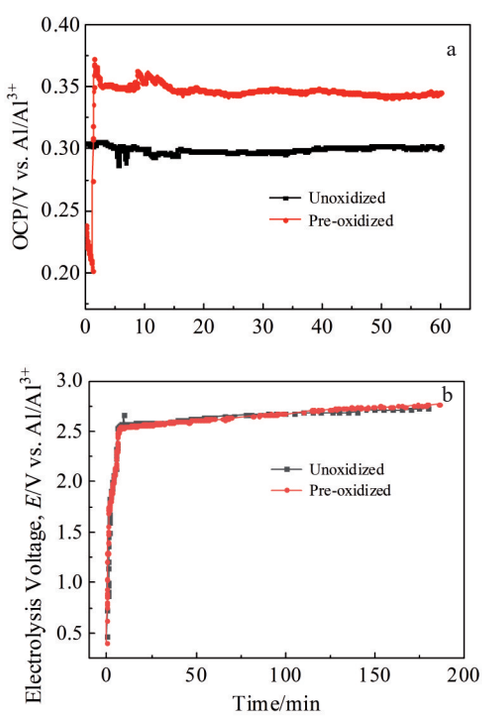


Fig.3 Variation of OCP for pre-oxidized and unoxidized anode alloys within the first hour of immersion in the electrolyte (a); electrolytic voltage as a function of time for pre-oxidized and unoxidized anode alloys (b)

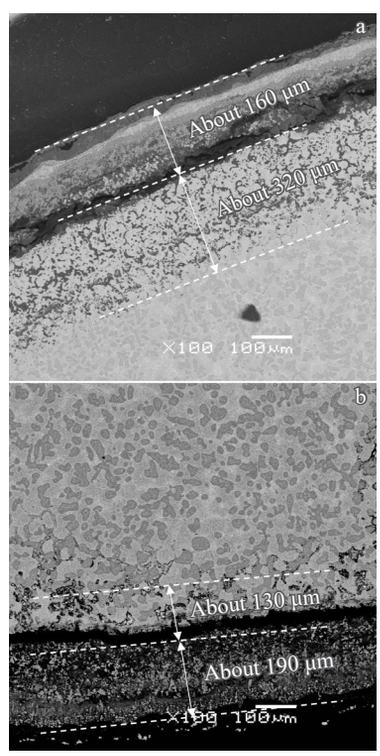


Fig.4 Cross-sectional SEM images of surface oxide layer of unoxidized (a) and pre-oxidized (b) 56Cu-22Ni-12Fe-8Al-2La anode alloys after electrolysis at 800 °C for 3 h

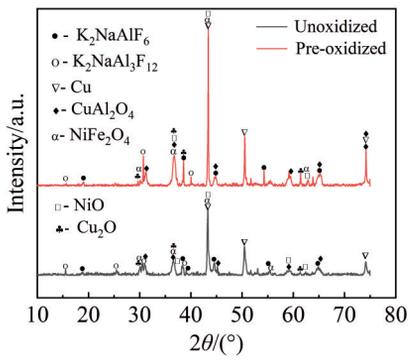


Fig.5 XRD patterns for oxide layers of unoxidized and pre-oxidized anode alloys after electrolysis at 800 °C for 3 h

thickness of approximately 320 μm. The electrolyte preferentially penetrates along La-rich regions toward the metal substrate. This is attributed to the fact that La can reduce the grain boundary energy at segregation sites and react with electrolyte ($La+AlF_3 \rightarrow LaF_3+Al$) during aluminum electrolysis[36]. The penetrated electrolyte may give rise to the microlocal corrosion of the metal anode, resulting in the degradation of the mechanical properties of the oxide layer, and even making the oxide layer easily exfoliated.

In contrast, for the pre-oxidized anode alloy, the oxide layer is about 190 μm-thick and also shows a tri-layered structure (Fig. 6b). Both the outer and inner oxide layers include dense and continuous Ni-/Fe-/Al-/Cu-rich oxides (mainly $NiFe_2O_4$ and $CuAlO_2$) with a small amount of electrolyte. The middle layer consists of a dense and continuous Ni-/Fe-rich oxide ($NiFe_2O_4$) with a thickness of about 15 μm. Apparently, the undamaged $NiFe_2O_4$ layer combined with the dense Ni-/Fe-/Al-/Cu-rich oxides (mainly $NiFe_2O_4$ and $CuAlO_2$) can offer superior corrosion resistance in cryolite-alumina molten electrolyte. The formation of a dense, continuous $NiFe_2O_4$ layer and a Ni-/Fe-/Al-/Cu-rich oxide layer may be attributed to the homogeneous microstructure resulting from the high-temperature pre-oxidized treatment. Moreover, the outward diffusion of Cu is restrained due to the homogeneous structure, and the formation of $NiFe_2O_4$ is promoted by the homogenization treatment[20]. It is worth noting that a small amount of F, Al, and K appears in the oxide layer and penetrates the metal matrix. The oxide layer formed on the pre-oxidized anode alloy exhibits better corrosion resistance and stability than that formed on the unoxidized anode alloy after aluminum electrolysis for 3 h. It is noted that delamination of oxide layer occurs for pre-oxidized anode alloy after electrolysis for 3 h. However, the whole oxide layer remains undamaged. Since only a little electrolyte is present in the Ni-/Fe-/Al-/Cu-rich oxides rather than filling the space between metal matrix and oxide layer, the oxide layer cannot delaminate during electrolysis. The delamination of oxide layer is probably due to the thermal shock when the metal anode is lifted above the molten electrolyte after electrolysis. Besides, the difference in the coefficients of thermal expansion between the alloy substrate and the oxide layer may also induce the delamination[31,37].

3.3 Corrosion mechanism of the unoxidized and pre-oxidized anode alloys

Fig. 7 shows the linear sweep voltammetry curves of the unoxidized and pre-oxidized anode alloys in the molten salt at

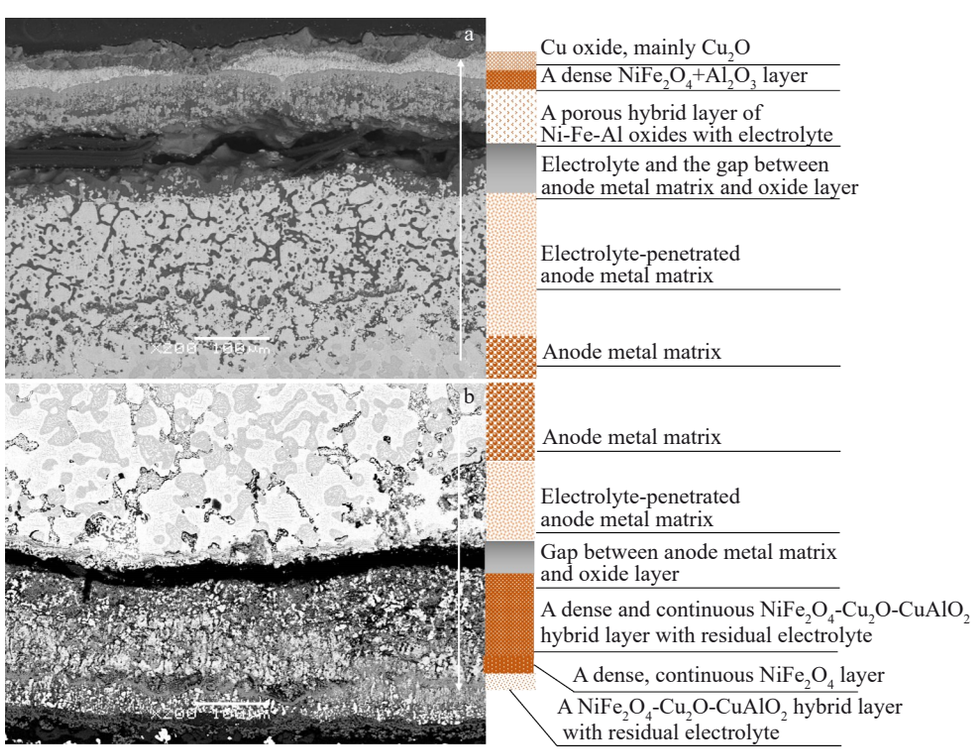


Fig.6 Microstructures and corresponding phase composition of surface oxide layer of unoxidized (a) and pre-oxidized (b) 56Cu-22Ni-12Fe-8Al-2La anode alloys after electrolysis at 800 °C for 3 h

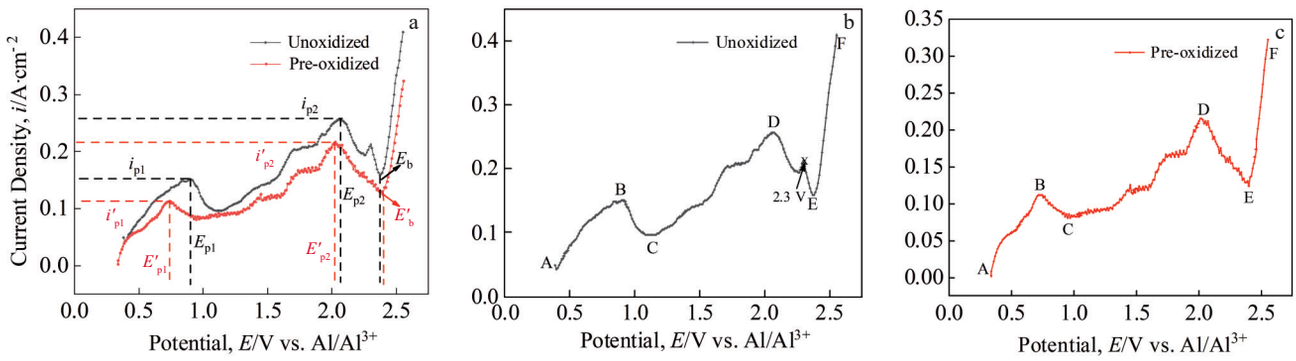


Fig.7 Comparison (a) and detailed analyses (b–c) of anodic polarization curves of unoxidized (b) and pre-oxidized (c) anode alloys in molten aluminum electrolysis at 800 °C

800 °C. The scanning range is from OCP to 2.8 V vs. Al/Al^{3+} at a scanning rate of 0.001 $V \cdot s^{-1}$. Obviously, the polarization current density of pre-oxidized anode alloy is slightly lower than that of unoxidized anode alloy, proving a little better corrosion resistance of the pre-oxidized anode alloy. The linear sweep voltammetry curves of both alloys are divided into four stages. In order to interpret the reaction occurring on the alloy surface at different potential ranges, the electromotive series for aluminum electrolysis at 1100 K are also calculated based on the Gibbs free energies of formation of compounds in JANAF thermochemical tables[15,38–39]. In the AB stage, the current density increases with a positive shift of the potential, indicating the alloy undergoes dissolution and reaction with the molten salt. This behavior corresponds to the active dissolution of the alloy, particularly the dissolution of La.

$La+F^{-} \rightarrow LaF_3$ E=0.71 V vs. Al/Al^{3+} (1)

BC and DE stages represent the passivation transition zones. The decreased current densities within the passivation transition zones are attributed to the transformation of metallic elements from the active state to the passivated state, resulting in the gradual formation of protective oxide layers on the anode surfaces. In CD stage, the current densities of both unoxidized and pre-oxidized alloys increase gradually, indicating the dissolution of the metallic elements at the specific potential[25]. The predominant reactions occurring at CD stage may involve the following reactions[40]:

$Fe+Al_2O_3 \rightarrow Fe_2O_3+Al$ E^0=1.37 V vs. Al/Al^{3+} (2)

$Ni+Fe+Al_2O_3 \rightarrow NiFe_2O_4+Al$ E^0=1.396 V vs. Al/Al^{3+} (3)

$Ni+AlF_3 \rightarrow NiF_2+Al$ E^0=1.71 V vs. Al/Al^{3+} (4)

$Cu+Al_2O_3 \rightarrow Cu_2O+Al$ E^0=1.84 V vs. Al/Al^{3+} (5)

$Cu+Al_2O_3 \rightarrow CuO+Al$ E^0=1.99 V vs. Al/Al^{3+} (6)

$Cu+AlF_3 \rightarrow CuF_2+Al$ E^0=2.06 V vs. Al/Al^{3+} (7)

$Al_2O_3+AlF_3 \rightarrow Al_xO_yF_z+Al$ E^0=2.07 V vs. Al/Al^{3+} (8)

$Cu_2O+Al_2O_3 \rightarrow CuO+O_2+Al$ E^0=2.25 V vs. Al/Al^{3+} (9)

$Cu+AlF_3 \rightarrow CuF_2+Al$ E^0=2.3 V vs. Al/Al^{3+} (10)

$Al_2O_3 \rightarrow Al+O_2$ E^0=2.351 V vs. Al/Al^{3+} (11)

However, it is noted that pre-oxidized alloy exhibits three distinct current plateaus in CD stage. This phenomenon is attributed to the homogenized microstructure induced by pre-oxidation, facilitating the formation of dense, continuous, and stable passive oxide layers at potentials between 0.73 V vs. Al/Al^{3+} and 2.09 V vs. Al/Al^{3+}. Comparatively, the current density for unoxidized anode alloy in CD stage continuously increases to about 1.7 V vs. Al/Al^{3+}, accompanied by the appearance of a slight current plateau. Besides, the peak current density observed at 2.3 V vs. Al/Al^{3+} for unoxidized alloy may be attributed to the formation of CuO and CuF_2, as shown in Eq. (9 – 10), indicating that the oxide layer formed via electrochemical polarization cannot effectively block fluoride ions from penetrating into the metal matrix. However, for pre-oxidized anode alloy, a better passive oxide layer formed during the electrochemical polarization process suppresses further penetration of fluoride ions and avoids the reaction between fluoride ions and the metal substrate at 2.3 V vs. Al/Al^{3+}. Finally, in EF segment, the alumina begins to decompose, with oxygen evolution starting at the breakdown potential (E_b, E'_b), and the current density increases with the increase in potential.

Additionally, the linear sweep voltammetry curves show several characteristic potentials and currents, which are important for evaluating the passivation behavior of alloys in molten salt. A more negative passivation potential (E_p, E'_p) indicates a greater tendency for the metal to enter the passivation state. Obviously, the E'_{p1} and E'_{p2} values of the pre-oxidized alloy are more negative than those of unoxidized alloy (E_{p1}, E_{p2}), indicating that the metal more readily enters the passivation state.

To further investigate the corrosion resistance of unoxidized and pre-oxidized anode alloys in the molten electrolyte, EIS tests were conducted after the OCP of the anode alloys stabilized in the molten electrolyte for approximately 1 h. The results are displayed in Nyquist and Bode plots in Fig. 8a–8c. For the metal corrosion, the Nyquist plot usually consists of three regions that are dependent on the frequency range. At high frequency, the non-zero intercept on the real axis indicates the equivalent series resistance (R_s) of a system, which mainly corresponds to the bulk resistance of the electrolyte. In the medium-frequency region, electrochemical behavior related to the interfacial charge transfer resistance of an electrode/electrolyte system is attributed to the capacitive behavior of the electrodes. The low-frequency region reflects the diffusion characteristics related to electrode porosity and

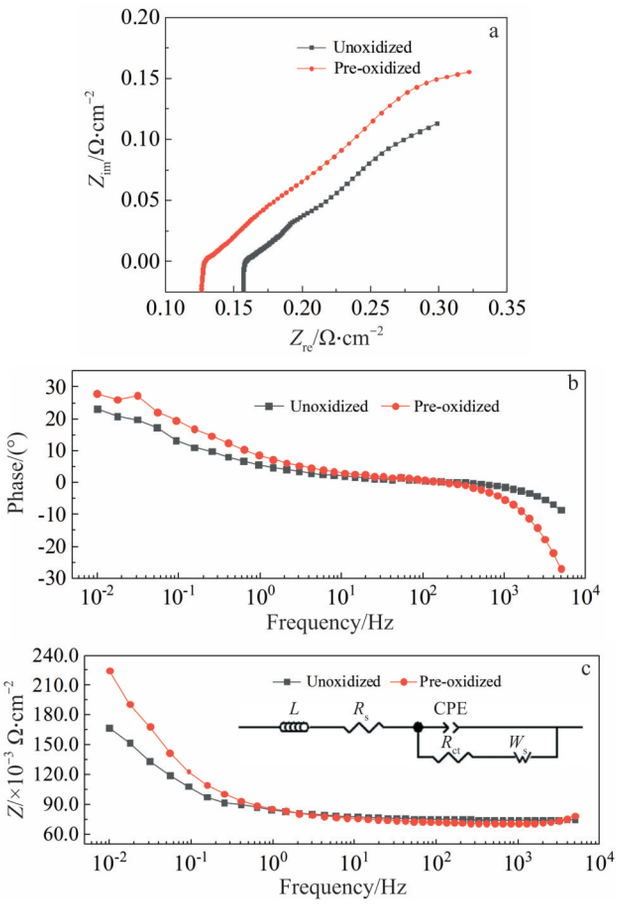


Fig.8 Nyquist plots (a) and Bode plots (b–c) of the unoxidized and pre-oxidized anode alloys after immersion in molten aluminum electrolysis at 800 °C for 1 h (the illustration in Fig.8c represents an equivalent circuit)

surface states. After immersion for 1 h, the Nyquist plots for both anode alloys feature a high-frequency R_s, a medium-frequency capacitive arc, and a low-frequency impedance arc with Warburg characteristics. To elucidate the corrosion process from EIS, the impedance spectra were fitted using the equivalent circuit in Fig.8c, where L represents the inductance, and R_s is the solution resistance. Considering that the corrosion interface of metal anodes may contain defects instead of forming an ideally smooth surface, an electrochemical effect exists at the metal/solution interface. A constant phase element (CPE) is commonly used to replace an ideal capacitor (C), R_{ct} is the charge transfer resistance, and W_s is Warburg impedance[41–43]. Table 1 summarizes the fitted equivalent circuit parameters.

A higher R_{ct} of the pre-oxidized alloy compared with that of the unoxidized anode alloy indicates that the oxide products formed by pre-oxidation on 56Cu-22Ni-12Fe-8Al-2La alloy may impede ion-substrate interactions at the initial immersion stage in molten electrolyte. Besides, the higher Warburg impedance of pre-oxidized alloy represents lower diffusion of the electrolyte into the pre-oxidized alloy surface. It is further confirmed that the pre-formed oxide film can provide partial barrier protection against electrolyte diffusion and corrosion attack on the metal substrate of the pre-oxidized anode alloy. EIS measurements of the unoxidized and pre-oxidized anode alloys with various galvanostatic electrolysis durations were also conducted. It is observed that the R_s gradually increases with the prolongation of galvanostatic electrolysis duration. However, the data at low frequencies exhibit irregularities originating from the evolution of oxygen bubbles during electrolysis.

Finally, it should be noted that long-term electrolysis or large current density may alter the performance of the 56Cu-22Ni-12Fe-8Al-2La anode alloy significantly. This study does not aim to screen the anode alloy for excellent long-term stability; instead, it aims to clarify the influence of pre-oxidation on the corrosion behavior of the 56Cu-22Ni-12Fe-8Al-2La alloy in the initial electrolysis stage.

Therefore, in the future, a long-term electrolysis should be conducted in a laboratory cell at 20 and 200 A for 24–72 h. If the metallic anode presents satisfactory performance in these tests, further electrolysis experiments at 20 kA will be conducted to systematically evaluate the anode electrochemical performance and the overall operating performance of the electrolysis cell. This study aims to provide reliable experimental data to support the industrial application of the developed metallic anodes.

4 Conclusions

1) The oxide layer formed on 56Cu-22Ni-12Fe-8Al-2La alloy at 800 °C under an O_2 atmosphere is mainly composed of oxides of Al, Ni, Fe, Cu, and La. In particular, the oxide of Al is the predominant product. To some extent, the formation of this oxide layer can prevent the rapid erosion of the metal anode by the electrolyte during the initial immersion period.

2) After aluminum electrolysis for 3 h, the oxide formed on the surface of the unoxidized 56Cu-22Ni-12Fe-8Al-2La anode alloy is composed of a tri-layered oxide structure with an outer layer of Cu oxide (mainly Cu_2O), a middle layer containing discontinuous $NiFe_2O_4$ and Al_2O_3, and an inner layer composed of porous Ni-/Fe-/Al-rich hybrid oxides. The discontinuous and porous oxide layer provides a connected channel during electrolysis, allowing direct electrolyte contact with the anode metal matrix, ultimately leading to the

Table 1 EIS parameters of unoxidized and pre-oxidized anode alloys after immersing in molten aluminum electrolysis electrolyte for 1 h

Anode alloy	L/×10^{-9} H	R_s/×10^{-3} Ω·cm^{-2}	R_{ct}/×10^{-3} Ω·cm^{-2}	C_{dl}/×10^{-3} F·cm^{-2}	Dispersion coefficient, β	W_s/×10^{-3} Ω·cm^{-2}·s$^{-0.5}$
Unoxidized	762.7	157.8	50.4	201.3	0.5599	130.6
Pre-oxidized	2052	128.2	68.2	230.9	0.6036	177.3

formation of electrolyte penetration zones with a thickness of approximately 320 μm. The electrolyte preferentially penetrates along La-rich regions toward the metal substrate. The penetrated electrolyte may give rise to the microlocal corrosion of the metal anode, resulting in the degradation of the mechanical properties of the oxide layer, and even making the oxide layer easily exfoliated.

3) For the pre-oxidized anode alloy, the oxide layer is about 190 μm-thick and also shows a tri-layered structure. Both the outer and inner oxide layers include dense and continuous Ni-/Fe-/Al-/Cu-rich oxides (mainly $NiFe_2O_4$ and $CuAlO_2$) with a small amount of electrolyte. The middle layer contains a dense and continuous Ni-/Fe-rich oxide ($NiFe_2O_4$) with a thickness of about 15 μm. A small amount of F, Al, and K appears in the oxide layer and penetrates into the metal matrix. The oxide layer formed on the pre-oxidized anode exhibits better corrosion resistance and stability than that formed on the unoxidized anode after aluminum electrolysis for 3 h.

References

1 Haupin W. *History of Electrical Energy Consumption by Hall-Hiroult Cells*[M]. Warrendale: The Metallurgical Society, 1986: 106

2 Ratvik A P, Mollaabbasi R, Alamdari H. *ChemTexts*[J], 2022, 8: 10

3 Desclaux P. *Metallurgical and Materials Transactions B*[J], 2001, 32: 743

4 Kvande H, Haupin W. *JOM*[J], 2001, 53: 29

5 Gallino I, Kassner M E, Busch R. *Corrosion Science*[J], 2012, 63: 293

6 Yang W J, Wang Y, Zhai H F *et al. Journal of Materials Science*[J], 2020, 55: 4065

7 Wang Zhaowen, Luo Tao, Gao Bingliang *et al. Rare Metal Materials and Engineering*[J], 2005, 34(1): 158 (in Chinese)

8 Tian Z L, Lai Y Q, Li Z Y *et al*. *JOM*[J], 2014, 66: 2229

9 Xiao H, Hovland R, Rolseth S *et al. Metallurgical and Materials Transactions B*[J], 1996, 27: 18

10 He H B, Wang Y, Long J J *et al*. *Transactions of Nonferrous Metals Society of China*[J], 2013, 23(2): 381

11 Shi Z N, Junli J L, Gao B L *et al*. *High Temperature Materials and Processes*[J], 2011, 30: 247

12 Morozov Y A, Yalunin V S. *RUDN Journal of Engineering Research*[J], 2022, 23: 15

13 Tian Z L, Lai Y Q, Yang S *et al*. *Metallurgical and Materials Transactions B*[J], 2015, 46: 1257

14 Sun F L, Li X G, Lu L *et al*. *Acta Metallurgica Sinica* (*English Letters*)[J], 2013, 26(4): 121

15 Beck T R, Macrae C M, Wilson N C. *Metallurgical and Materials Transactions B*[J], 2011, 42: 807

16 Yasinskiy A S, Padamata S K, Polyakov P V *et al*. *Transactions of Nonferrous Metals Society of China*[J], 2020, 30(5): 1419

17 Sai K P, Andrey S Y, Peter V P. *Journal of Siberian Federal University Chemistry*[J], 2018, 11: 18

18 Liu Y, Chai D P, Wang W *et al*. *Journal of Alloys and Compounds*[J], 2020, 832: 154848

19 Helle S, Brodu B, Davis B *et al*. *Corrosion Science*[J], 2011, 53: 3248

20 Guan P P, Li A M, Shi Z N *et al*. *Metals*[J], 2019, 9(4): 399

21 Huang Y P, Yang Y J, Zhu L M *et al*. *International Journal of Electrochemical Science*[J], 2019, 14: 6325

22 Shi Z N, Xu J L, Qiu Z X *et al*. *JOM*[J], 2003, 55: 63

23 Zhuravleva E N, Drozdova T N, Ponomareva S V *et al. Applied Surface Science*[J], 2013, 265: 790

24 Cao D, Ma Y F, Shi Z N *et al. Corrosion Science*[J], 2019, 156: 3

25 Helle S, Davis B, Guay D *et al*. *Journal of the Electrochemical Society*[J], 2010, 15: E173

26 Yang W J, Guo J, Li J *et al. Journal of the American Ceramic Society*[J], 2017, 100: 887

27 Wei W, Geng S J, Wang F H. *Journal of Materials Science & Technology*[J], 2022, 107: 216

28 Tamasgavabari R, Jafarzadeh K, Madanipoor M *et al*. *Anti-Corrosion Methods and Materials*[J], 2015, 62: 1

29 Singh K, Gunnarsson G, Magnusson J H *et al*. *Journal of the Electrochemical Society*[J], 2023, 170: 113507

30 Liu Y, Zhang Y A, Wang W *et al. Arabian Journal for Science and Engineering*[J], 2018, 43: 6285

31 Wei W, Geng S J, Xie D B *et al. Corrosion Science*[J], 2019, 157: 382

32 Liu Ying, Liang Zhimin, Wang Liwei *et al*. *Journal of Hebei University of Science and Technology*[J], 2021, 42(3): 296 (in Chinese)

33 Goupil G, Helle S, Davis B *et al*. *Electrochimica Acta*[J], 2013, 112: 176

34 Goupil G, Jucken S, Poirier D *et al*. *Corrosion Science*[J], 2015, 90: 25

35 Helle S, Tresse M, Davis B *et al*. *Journal of the Electrochemical Society*[J], 2012, 15: E62

36 Zhang P Y, Liu Z, Liu Z H *et al. Special Casting & Nonferrous Alloys*[J], 2024, 44: 271

37 Church B C, Sanders T H, Speyer R F *et al. Materials Science and Engineering A*[J], 2007, 452–453: 334

38 Stull D R, Prophet H. *JANAF Thermochemical Tables*[M]. Washington: U.S. National Bureau of Standards, 1971

39 Padamata S K, Yasinskiy A, Shabanov A *et al*. *Transactions of Nonferrous Metals Society of China*[J], 2022, 32(1): 354

40 Qian Xukun, Zhu Chuncheng, He Xiaodong. *Rare Metal Materials and Engineering*[J], 2007, 36(11): 1979 (in Chinese)

41 Alzamani M, Jafarzadeh K, Fattah-Alhosseini A. *Materials and Corrosion*[J], 2019, 70: 605

42 Zeng C L, Wang W, Wu W T. *Corrosion Science and Protection Technology*[J], 2000, 12: 249

43 Ni C S, Lu L Y, Zeng C L *et al*. *Corrosion Science*[J], 2011, 53: 1018

预氧化56Cu-22Ni-12Fe-8Al-2La阳极在铝电解高温熔盐电解质中的腐蚀行为

杜　娟[1,2]，包生重[3]，杨少丹[1,2]，周延军[2,4]，庄玉伟[5]，曹书光[1]

（1. 河南省科学院 材料研究所，河南 郑州 450046）

（2. 河南省先进导体材料重点实验室，河南 郑州 450002）

（3. 中铝郑州有色金属研究院有限公司，河南 郑州 450041）

（4. 河南科技大学 材料与工程学院，河南 洛阳 471000）

（5. 河南省科学院高新技术研究中心，河南 郑州 450046）

摘　要：研究了未氧化和预氧化的56Cu-22Ni-12Fe-8Al-2La阳极合金在800 ℃的Na_3AlF_6-K_3AlF_6-AlF_3-Al_2O_3铝电解用熔盐电解质中的腐蚀行为。测试了金属阳极在铝电解熔盐中的电化学性能，并研究了合金的腐蚀机理。结果表明，合金在800 ℃、O_2气氛下预氧化形成的氧化层主要由含铝、镍、铁、铜和镧元素的氧化物组成。电解3 h后，未氧化的金属阳极形成的腐蚀产物呈三层结构，腐蚀产物中不连续且多孔的氧化层在电解过程中提供了连通通道，使电解质易直接渗透进入金属基体，深度约为320 μm；预氧化后的金属阳极形成的腐蚀产物氧化层厚度约为190 μm，外层和内层氧化层包含连续的富Ni/Fe/Al/Cu氧化物（主要为$NiFe_2O_4$、$CuAlO_2$），中间层为致密连续的$NiFe_2O_4$层，厚度约为15 μm，氧化层中出现少量电解质，并渗入金属基体。在铝电解过程中，预氧化后的合金较未氧化的金属阳极合金表现出更优的耐腐蚀性能和稳定性。

关键词：Cu-Ni-Fe-Al-La合金；金属阳极；高温熔盐腐蚀；铝电解

作者简介：杜 娟，女，1982年生，博士，正高级工程师，河南省科学院材料研究所，河南 郑州 450046，E-mail：juan_du@hnas.ac.cn